AIAA JOURNAL
Vol. 34, No. 6, June 1996

Forward Motion Effects on Jet Noise, Panel Vibration, and Radiation

A. Bayliss*
Northwestern University, Evanston, Illinois 60208
L. Maestrello†
NASA Langley Research Center, Hampton, Virginia 23681-0001
J. L. McGreevy‡
Philadelphia College of Pharmacy and Science, Philadelphia, Pennsylvania 19104
and
C. C. Fenno Jr.§
National Research Council, Hampton, Virginia 23681-0001

A model of the interaction of sound from a spreading subsonic jet with a four-panel assembly is studied numerically in two dimensions. The effect of forward motion of the jet is allowed for by considering a uniform flowfield superimposed on a mean jet exit profile. The jet is initially excited by a pulselike source inserted into the flow field. The pulse triggers instabilities associated with the inviscid instability of the jet shear layer. These instabilities generate sound, which in turn serves to excite the panels. The far-field acoustic radiation, the panel response, and the sound radiated from the panels are all computed and compared with computations with a static jet. The results demonstrate that for a jet in forward motion there is a reduction in sound in downstream directions and an increase in sound in upstream directions, in agreement with experiments. Furthermore, the panel response and radiation for a jet in forward motion exhibit a downstream attenuation as compared with the static case.

Introduction

THIS paper describes a numerical simulation of jet noise in the presence of four flexible aircraft-type panels in a panel–stringer assembly. The simulation is based on a model that fully couples the fluid dynamics of the jet flow to the panel motion and the resulting acoustic radiation, while allowing for the forward motion of the jet. The primary objective of this paper is to determine the role played by forward motion of the jet and the structure on installation effects.

In previous work[25] we have computed the far-field sound, panel response, and radiation from a static jet with a two-panel model. The acoustical behavior of a static jet is not sufficient to determine the behavior for a jet in flight. The noise radiated from the jet in the downstream direction should decrease with an increase in the forward velocity, because of the reduced shear resulting from the lower relative velocity between the jet and its surroundings. The effect of forward motion on panel response and radiation has not yet been completely determined. We describe here the effect of forward motion on the response and radiation of the panels. We note that the results presented here do not include the effect of the boundary layer on panel excitation. For any particular parameter range, the boundary layer may result in enhanced loading with increasing forward velocity.

The problem of simulating the behavior of a jet in flight has previously been studied analytically and experimentally. Analytic methods have included formulation of the exact sources (e.g., Refs. 19, 30), models of the sources to include flow effects (e.g., Refs. 12, 19), and analysis of the effects of moving sources (e.g., Refs. 1, 28). These analyses demonstrated reduction in noise emission downstream of the jet and generally an amplification in the forward direction.

There have also been extensive experimental studies of forward-motion effects. Measurements on a moving structure, the Bertin Aérotrain, were reported in Ref. 11. These results, obtained for locations fixed on the ground, showed a general reduction in level along the jet axis, but under certain conditions there was sound amplification in forward directions. Measurements of a jet in flight are reported in Ref. 8. Wind-tunnel measurements, in which the forward-motion effect is simulated by coflowing airstreams and measurements are taken at points fixed with respect to the jet, have also been obtained.[29,32]

An important feature of our model is the direct computation of at least some of the natural sources of jet noise, namely fluid-dynamical instability waves that arise from the instability of the jet shear layer. Experiments have demonstrated the existence of large-scale structures or instability waves in jets.[7,9,18,23,31] These structures are believed to act as sources of sound, a point also confirmed by analytical studies[6,17,27,26] and computations.[2,3,23] Our model allows the computation of panel response and radiation employing consistent sources (i.e., no additional modeling of the sources is required). We note that other approaches to panel response involve obtaining the forcing from experimental measurements, or modeling self-consistent forces (e.g., Ref. 10). Panel response and radiation are fully coupled to the fluid dynamics of the jet flow. Experiments have demonstrated that panel response and radiation are very heavily influenced by the nature of the forcing, i.e., by the sound from the jets.[22] Thus it is important that any simulation capture the essential features of the jet-noise forcing on the panels.

Problem Formulation

The computational domain is shown in Fig. 1. The Euler equations are solved in two domains separated by a wall containing four adjacent, rigidly clamped, flexible panels (panels 1–4 in Fig. 1). The jet domain contains the jet, exiting from a nozzle of width $D = 5.08$ cm, together with associated sources of sound. The panels are excited by sound generated from the jet and radiate sound into both domains. The radiation domain simulates the aircraft cabin. Panel radiation is studied by analyzing the unsteady pressure in the radiation domain (panel radiation into the jet domain is small compared to acoustic disturbances generated from the jet).

Received May 6, 1995; revision received Dec. 6, 1995; accepted for publication Dec. 11, 1995.

*Professor, Department of Engineering Sciences and Applied Mathematics.
†Senior Staff Scientist. Associate Fellow AIAA.
‡Assistant Professor, Department of Mathematics and Physics.
§Research Associate. Member AIAA.

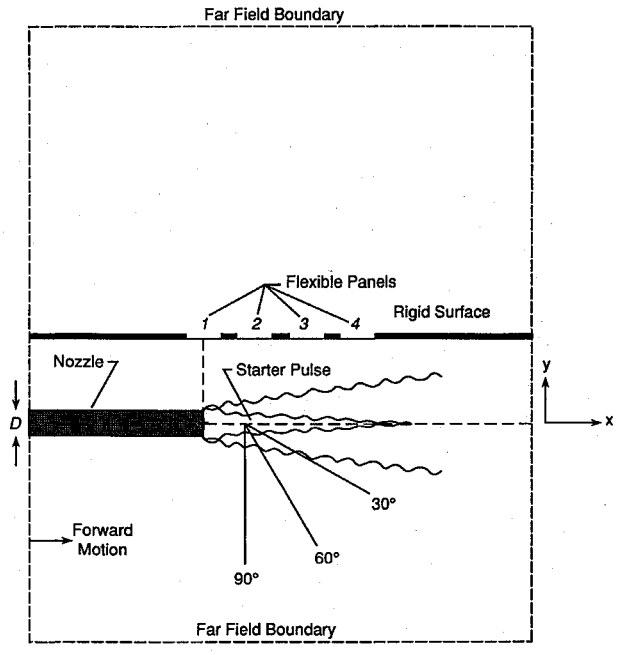

Fig. 1 Computational domain.

The computations involve coupling the solution of the Euler equations in the two domains to the nonlinear beam equation:

$$D_b \frac{\partial^4 z}{\partial x^4} - N_x \frac{\partial^2 z}{\partial x^2} + \rho_b h \frac{\partial^2 z}{\partial t^2} + \delta \frac{\partial z}{\partial t} = p^+ - p^- \qquad (1)$$

where z is the beam transverse deflection, ρ_b the mass per unit volume of the beam, h the beam thickness, and δ the physical damping. The stiffness of the beam is given by $D_b = Mh^3/12(1-\nu^2)$, where M is the modulus of elasticity, ν the Poisson ratio of the beam material, and N_x represents nonlinear bending.[25,13] Equation (1) is fully coupled to the fluid dynamics in that at each time step the pressure difference across the panels, $p^+ - p^-$, computed from the Euler equations, serves as a forcing term for the beam equation, while z_t, obtained from Eq. (1), is imposed as a boundary condition for the Euler solution. The major approximation made in formulating the coupled model is that of small displacement relative to the acoustic wavelength (e.g., Euler grid size), so that in the Euler code the panel location is taken as the horizontal line $y = 0$. Equation (1) is updated using a scheme similar to that in Ref. 16.

Each panel is of length $5D$ and thickness $0.01D$, and the panels are centered at $x = 0D$, $5.22D$, $10.44D$, and $15.66D$, respectively. We refer to the panels as panels 1, 2, 3, and 4 where panel 1 is the farthest upstream. Other parameters of the panels are typical of aluminum.

The Euler equations can be written in the form

$$\boldsymbol{w}_t + \boldsymbol{F}_x + \boldsymbol{G}_y = s_1(t, x, y) + s_2(x, y) \qquad (2)$$

with $\boldsymbol{w} = (\rho, \rho u, \rho v, E)^T$, where ρ is the density, u and v are the components of the velocity in the x and y directions, respectively, and E is the total energy per unit volume. The pressure, p, used to get the internal energy component of E, is obtained from the equation of state. The flux functions $\boldsymbol{F}$ and $\boldsymbol{G}$ are standard. The source terms s_1 and s_2 are described below. The Euler equations (2) are solved separately in both the jet and radiation domains, using the explicit 2–4 MacCormack scheme[14] together with operator splitting. The scheme is discussed in detail in Ref. 23.

In the jet domain we assume a straight pipe of width D from which the jet exits. The system (2) is modified to include two different source terms. The first term,

$$s_1(t, x, y) = \epsilon f(t) g(x, y) \boldsymbol{w}_I \qquad (3)$$

serves as the starter pulse to excite the jet by localized, transient mass injection. Here, ϵ describes the amplitude of the source, $f(t)$ is a short-duration pulse, and $g(x, y)$ is a Gaussian localized at the specified position (x_s, y_j), where y_j is the jet axis (approximately $6D$ from the wall); $x_s = 1.15D$, so that the starter pulse is in the potential core of the jet; and

$$\boldsymbol{w}_I = \{1, U_0, 0, [\gamma/(\gamma-1)]p_\infty\}^T$$

where the subscript ∞ denotes ambient quantities, $U_0(x, y)$ is a model describing a spreading jet profile taken from Ref. 21 in Cartesian coordinates, and γ is the ratio of specific heats. This vector is chosen as follows. The component in the continuity equation serves as a mass injection. This is balanced by the component in the energy equation, so that in the absence of flow and boundaries the solution remains homentropic. The component of the starter pulse in the axial momentum equation ensures that momentum is added to the system as the mass injected is convected downstream by the flow. An alternative approach, involving time-harmonic excitation of the jet, is described in Ref. 24. In the absence of flow and bounding surfaces, the solution would be a circular wave. We have verified this as part of the validation of the code and grid.

The pulse $f(t)$ is chosen so that without any flow the peak frequency of the far-field pressure is close to 1000 Hz. The pulse strength ϵ is $1.0/f_{\max}$, where $f_{\max}$ is the maximum of $f(t)$.

The second source term $s_2(x, y)$ is designed so that in the absence of the starter pulse, i.e., $\epsilon = 0$, the solution to Eq. (2) would be a stationary profile corresponding to a spreading jet:

$$\boldsymbol{w}_0 = \left(\rho_\infty, \rho_\infty U_0, 0, \rho_\infty U_0^2/2 + c_v \tilde{T}_\infty\right)^T$$

In the limit of small ϵ, the term s_2 leads to the Euler equations linearized about a spreading jet, as in Ref. 23, which by itself need not be a solution to the Euler equations. Incorporation of this term within the nonlinear Euler equations allows for the computation of nonlinear disturbances within the mean jet profile as in Ref. 3. The inclusion of this source term separates the computation of the disturbance, in particular the resulting instability waves, from the computation of the mean flow (i.e., the spreading jet). Thus, the resulting system of equations allows for the simulation of instability waves and the resulting sound generation, together with the bending of acoustic waves in the jet flowfield, without requiring the computation of the spreading jet itself. Although this is a simplified model, it captures many of the observed features of instability-wave-generated jet noise and permits high-resolution computation of the coupling of jet noise with the flexible panels and the resulting radiation from the panels. In particular, the model allows for computation of the natural sources of jet noise (the instability waves) together with the sound radiated by these sources.

The initial conditions are $\boldsymbol{w}_0$ in the jet domain and ambient data in the radiation domain. The boundary conditions are as follows (refer to Fig. 1):

1) *Bounding wall*: rigid conditions except for the flexible panels, which are treated as described above.

2) *Pipe*: rigid on interior, impedance on exterior. The use of impedance boundary conditions on the exterior of the pipe simulates the use of an absorbing material to absorb waves incident on the pipe from the exterior.

3) *Inflow for the pipe*: characteristic conditions that are nonreflecting on the lowest propagating mode in the pipe.[23] The boundary condition can lead to reflections on higher modes; however, any such reflections do not effect the data outside the pipe for the time intervals considered here.

4) All other boundaries in the problem are artificial. Nonreflecting (radiation) boundary conditions are imposed to prevent spurious reflections from propagating into the interior.

We describe in more detail the treatment of the artificial boundaries. When there is no forward motion, one boundary condition must be prescribed at each boundary. The pressure in the far field is governed by the two-dimensional wave equation, which admits a far-field expansion in terms of powers of r, the distance from the origin of the region of sound generation. At these boundaries, we impose conditions designed to absorb outgoing circular waves.[4,5]

Specifically, we consider the leading term in the far-field expansion for $\tilde{p} = p - p_\infty$,

$$\tilde{p}(t, x, y) \approx \frac{d(c_\infty t - r, \theta)}{\sqrt{r}} \tag{4}$$

where r and θ are polar coordinates from a specified origin (taken as the location of the starter pulse) and c_∞ is the ambient sound speed. Differentiation of Eq. (4) with respect to t and r results in the relation

$$\tilde{p}_t + c_\infty \tilde{p}_r + \tilde{p}/2r = O\left(r^{-\frac{3}{2}}\right) \tag{5}$$

Neglecting the right-hand side of Eq. (5) results in a radiation boundary condition that is effective in simulating outgoing waves, provided the boundaries are sufficiently distant from all sources.[4,5] We have verified that there are negligible boundary reflections for the data presented in this paper.

For the computation with forward motion, it is necessary to consider a far-field expansion of the convective wave equation. Such an expansion has been carried out in Ref. 5, where boundary conditions based on the leading term in the expansion are derived. We employ these boundary conditions at our artificial boundaries [specifically, Eq. (23) in Ref. 5]. A comparison of different boundary conditions in Ref. 15 has demonstrated the effectiveness of this methodology. There are negligible boundary reflections for the forward-motion computation presented in this paper.

When there is forward motion, two additional boundary conditions should be imposed at inflow. We impose the conditions $c_\infty \rho - p/c_\infty = c_\infty \rho_\infty - p_\infty/c_\infty$, $u_y - v_x = 0$, simulating isentropy and irrotational flow at inflow. For the values of the forward motion considered here these boundary conditions have a negligible effect on the solution.

Finally, we outline the steps involved in advancing the solution one timestep.

1) Equations (2) are advanced one time step in both the jet domain and the radiation domain. Boundary conditions are not imposed; however, temporary variables on the boundaries are obtained using third-order extrapolation of the flux functions. We note that in the jet domain, Eq. (2) is solved in both the interior and exterior of the pipe (see Fig. 1).

2) Using the temporary boundary values, the pressure difference across the panels is computed.

3) Equation (1) is advanced one time step using the computed pressure difference across the panels as a source term.

4) The normal velocity on the panels is computed.

5) The computed normal velocity is then used as a boundary condition for Eq. (2), for both the jet domain and the radiation domains.

6) The remainder of the boundary conditions for the jet domain and radiation domain are imposed.

7) Go back to step 1 to update to the next time level.

Results

The origin of coordinates is chosen to be the horizontal location of the nozzle exit for x and the vertical location of the rigid wall for y. Both the jet and radiation domains extend $48D$ downstream from $x = 0$, $36D$ in the upstream direction, and $48D$ in the y direction. We employ a grid of 811×501 points in the jet domain and 441×301 points in the radiation domain. The grid in the jet domain is stretched to improve resolution of the jet shear layer and source region. The grid in the radiation domain is uniform. The computations have been validated by grid refinement. Examples of such grid refinements are given in Ref. 25. Based on grid refinements, we believe that there are no significant numerical errors for the data presented here.

We consider two computations. In the static computation we assume a static jet with exit velocity $U_j = 0.65c_\infty$. In the forward-motion computation we model a forward motion effect with a uniform flow of speed $U_f = 0.20c_\infty$ in the x direction superimposed on the jet mean flow. The Mach number for the mean jet profile is 0.45, so that the exit velocity from the nozzle is still $0.65c_\infty$, but the jump in velocity across the jet boundary is now $0.45c_\infty$. This models a wind-tunnel experiments of forward-motion effects. We compute the sound at points that are fixed with respect to the jet, simulating measurements at a fixed location in a wind tunnel.

Our results are presented in three parts: the jet domain, including the flow and acoustic radiation from the jet; the responses of the panels; and the acoustic radiation from the panels.

Jet Flow Domain

Nonstationary behavior in the jet is triggered by the starter pulse, which generates a disturbance that propagates through the jet, interacts with the shear layer, and then propagates into the far field as sound. This disturbance is noncircular because of the flow. Additional disturbances due to purely geometric effects, such as reflection from the wall and scattering from the nozzle lip, are also generated. In addition, instability waves are generated as a result of the interaction of the acoustic disturbance with the shear-layer gradient of the jet profile.

After an initial growth, the amplitude of the instability waves decays because of the spreading of the mean velocity. As they propagate downstream, they act as sources of disturbances, which propagates into the far field as sound.[19,20,26,27,30] These disturbances also trigger additional disturbances from the nozzle lip via a feedback mechanism, leading to a sustained response of the jet. This behavior is also consistent with experimental observations[6,9] and with previous linear and nonlinear computations.[2,3,23] The resulting sound radiation forces the panels into a broadband, sustained response, which in turn leads to a sustained radiation of sound from the panels. The acoustic radiation persists after the initial disturbance generated by the starter pulse has propagated away from the region of interest.

We examine $\tilde{p}$ at given far-field locations and also over the restricted interval $10 \le t \le 20$ to eliminate the effect of the starter pulse and focus on the sound generated from the instability waves in the jet. Changing the selected interval leads to quantitative changes but does not change the qualitative pattern of the far-field sound. Examination of the starter pulse permits a study of the effect of forward motion on wave propagation through the jet and generation of instability waves, and examination of the long-time behavior permits a study of sound generation from the instability waves.

It is known that over a wide range of parameters the intensity of jet noise exhibits a midangle peak.[18,31] It has also been observed and predicted that forward motion leads to a reduction in sound downstream of the jet and an increase in sound in the upstream direction (i.e., a forward arc amplification, e.g., Refs. 11, 28). We illustrate this in Fig. 2a, where we plot the logarithm of the time-integrated intensity, $\tilde{I} = 10 \log_{10}[\int_{t_1}^{t_2} \tilde{p}^2 \, dt/(t_2 - t_1)]$, with $t_1 = 0$ and $t_2 = 20$,

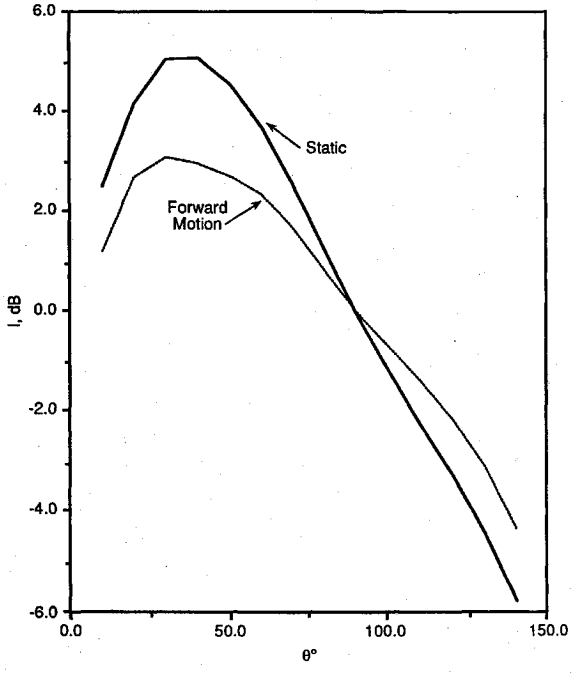

Fig. 2a Intensity of far-field sound for computations with and without forward motion. Data taken on a circle of radius 30D.

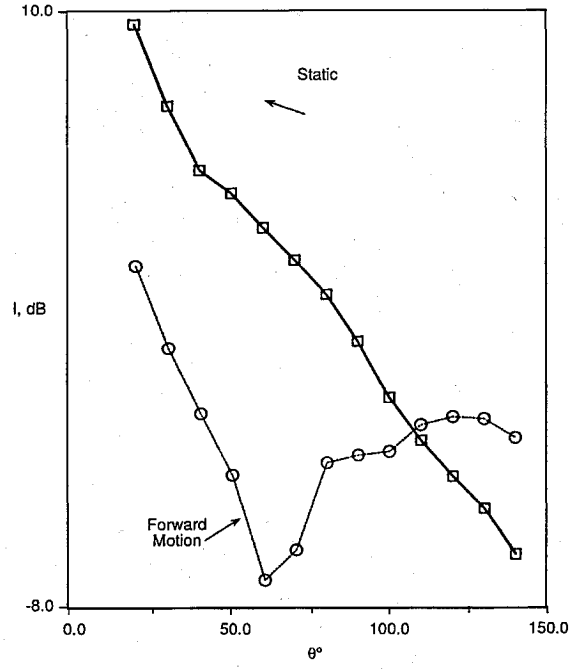

Fig. 2b Intensity of far-field sound for computations with and without forward motion. Data taken on a circle of radius 30*D*. Long-time behavior of pressure field considered.

around a circle of radius $30D$ from the starter-pulse location. The decibel level is normalized to 0 for the static computation at 90 deg. The results clearly demonstrate the downstream attenuation of sound and upstream amplification, in qualitative agreement with experiments and analysis. The crossover angle is very close to 90 deg.

In Fig. 2b we plot that analogous graph for $t_1 = 10$ and $t_2 = 20$, thus examining the effect of forward motion on sound generated from the jet due to instability waves. The data are again normalized so that 0 dB is at 90 deg for the static computation. We note that the qualitative effect of forward motion is similar: there is a reduction along the jet axis and a forward arc amplification. There are now significantly larger differences between the computations with and without forward motion, indicating a significant effect of forward motion in reducing sound generation from instability waves.

In summary, these plots indicate that the observed properties of forward motion, namely a reduction in observed sound downstream and an amplification upstream, can be explained as both a wave propagation effect, as evidenced by the behavior shown in Fig. 2a, accounting for the total pressure field, and as a sound generation effect, as shown in the long-time behavior in Fig. 2b.

In Fig. 3a we plot the time histories of the $\tilde{p}$ at 30, 60, and 90 deg along the same far-field arc considered in Figs. 2a and 2b. The graphs show the leading acoustic disturbance, a secondary disturbance resulting from reflections from the wall, and additional sound generated at later times from the instability waves. The latter are particularly noticeable at 30 deg for the static computation. The graphs clearly show the midangle amplification of sound resulting from the flow. There is amplification for both the starter pulse and the later arrivals. The downstream attenuation of sound with forward motion can be most readily seen from the data at 30 deg. Both the leading pulse and the later arrivals resulting from instability waves are attenuated, suggesting that this is largely a wave propagation phenomenon.

In Fig. 3b we plot the spectrum $|\hat{p}(\omega)|$, where

$$\hat{p}(\omega) = \int_0^T [p(t) - p_{\text{mean}}] \exp(-i\omega t)\, dt/T$$

at 30 and 90 deg as a function of the frequency $f = 2\pi\omega$. In this figure, as in other spectral plots, T is 15 in nondimensional units and p_{mean} is the mean of $p(t)$ over the indicated time interval. The data are presented in terms of dimensional frequencies (i.e., in hertz), to indicate the range of frequencies considered in our computations. The data are normalized by the maximum over both angles. The effect of forward motion is an overall attenuation, particularly at low frequencies, at 30 deg. The effect of forward motion is barely seen at 90 deg for all frequencies and also for high frequencies at 30 deg. Figures 3a and 3b illustrate the role of the jet as an amplifier of sound at low to midrange angles and the effect of forward motion in reducing this amplification.

The spectrum at 30 deg is qualitatively similar to spectra that have been computed and measured previously (e.g., Ref. 25) without the presence of the wall. In contrast, certain features of the spectrum, particularly at large angles (e.g., 90 deg), are primarily geometrical in nature, because of interference between the direct arrival and the reflected wave from the wall. This can be seen by comparing Fig. 3b with analogous data for the static jet at 90 deg presented in Ref. 25.

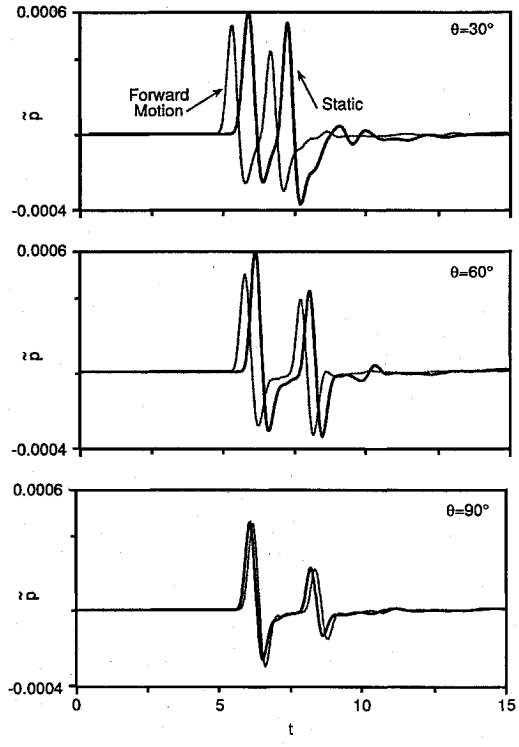

Fig. 3a Time histories of $\tilde{p}$ at angles of 30, 60, and 90 deg on a circle of radius 30*D*.

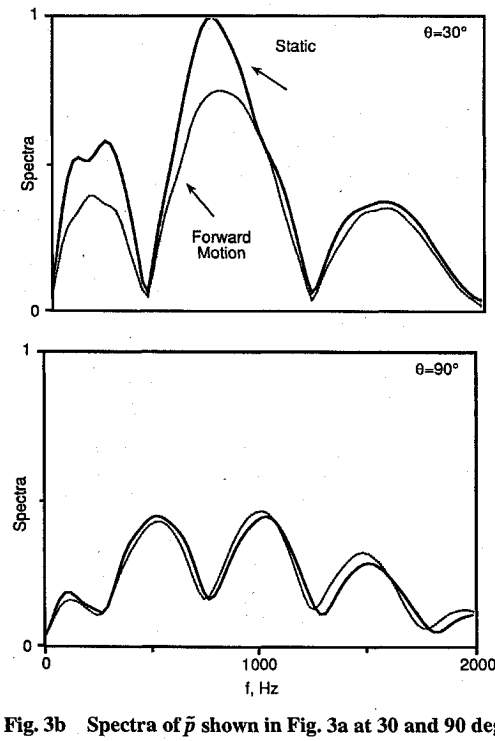

Fig. 3b Spectra of $\tilde{p}$ shown in Fig. 3a at 30 and 90 deg.

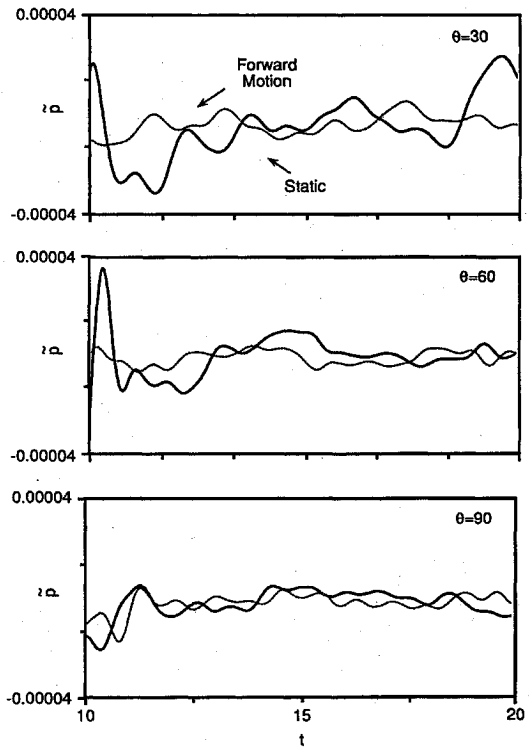

Fig. 3c Time histories of $\tilde{p}$ at angles of 30, 60, and 90 deg on a circle of radius 30D. Data presented only over the interval $10 \leq t \leq 20$ after starter pulse has passed away from selected points.

In Fig. 3c we illustrate the long-time behavior of $\tilde{p}$, after the starter pulse has passed away from the selected points. Since the total intensity is measured by the integral of $\tilde{p}^2$, the results demonstrate the additional sound generated in the static case for 30 and 60 deg.

In summary, the results show the following:

1) The jet acts as an amplifier of sound, primarily at low to midrange angles to the jet axis.

2) There is amplification both for the primary wave (a wave propagation effect) and for the later arrivals, illustrating sound generated from instability waves in the jet.

3) The effect of forward motion is most noticeable in attenuating low frequencies for low to midrange angles downstream.

4) The installation effect (i.e., forward motion, reflections from the wall and coupling between the wall and the jet) significantly alters the spectrum of the far-field sound, particularly for low- to midrange angles.

5) There is virtually no effect of forward motion at angles approaching 90 deg.

Panel Response

We categorize the panel response by considering 1) $\tilde{p}$ incident on the panels, 2) the velocities of the panels, and 3) the transmitted $\tilde{p}$. In each case we consider both time histories and spectral data at the center of the panel.

In Figs. 4a and 4b we consider $\tilde{p}$ in front of the panels on the jet side and at the panel centers for panels 1 and 2 (Fig. 4a) and panels 3 and 4 (Fig. 4b). Although these data include the effect of radiation from the panel into the jet domain, this is small compared to the incident $\tilde{p}$, and we refer to this quantity as the incident $\tilde{p}$. All graphs are plotted on the same scale. The effect of convection can be seen in that for panel 1 (upstream of the starter pulse) the primary arrival is slightly delayed with forward motion, whereas for the other panels the primary arrival is advanced with forward motion. The time difference between the leading arrivals with and without forward motion increases with distance of the panel from the starter pulse location. There is a slight increase in level for panel 1 (consistent with the forward arc amplification observed in Fig. 2a). There is an overall reduction in level for the primary arrivals for the downstream panels, again consistent with the downstream attenuation due to forward motion.

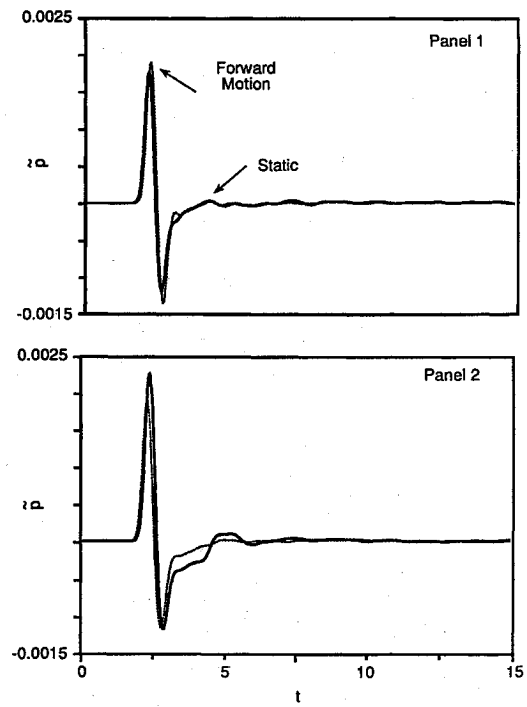

Fig. 4a Time history of incident $\tilde{p}$ for panels 1 and 2 at the panel centers, with and without forward motion.

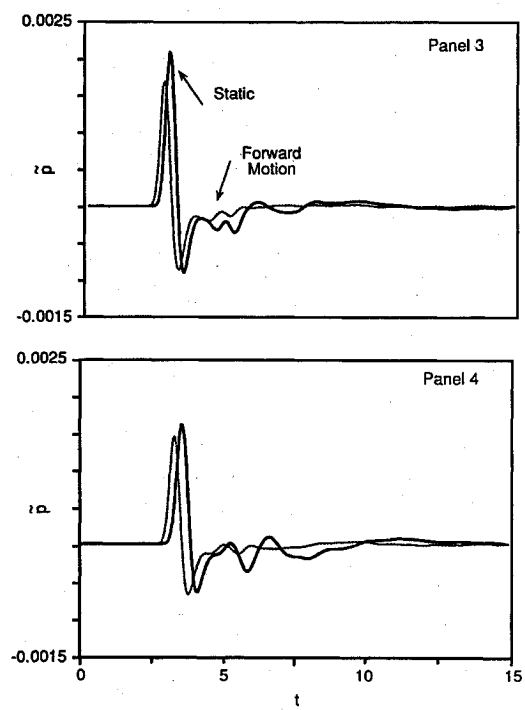

Fig. 4b Time history of incident $\tilde{p}$ for panels 3 and 4 at the panel centers, with and without forward motion.

Only very weak additional arrivals are observed for panel 1. In previous calculations we have found that panel 1 is only weakly influenced by sound from the instability waves. Rather, the primary loading of panel 1 is the result of repeated reflections between the nozzle and the panel. In the present computations we have employed impedance conditions on the exterior surface of the pipe to deemphasize this effect.

The effect of additional arrivals, resulting from additional sound generated from instability waves, can be seen first for panel 2 and becomes more pronounced for panels 3 and 4. The time duration of these additional arrivals increases with the downstream distance of the panels, suggesting panel excitation at lower frequencies, which is confirmed by analysis of the spectra. It is clear from the figures that the amplitude of these additional arrivals is reduced by forward

motion. Furthermore, the amount of the reduction increases with the downstream distance of the panels.

Analysis of the spectra of the incident $\tilde{p}$ indicates a rapid rolloff of high frequencies as the downstream distance of the panel increases. Thus the spectrum is more concentrated at lower frequencies as the downstream distance of the panel increases, consistent with the time histories in Figs. 4a and 4b. Furthermore, the low frequencies are significantly enhanced as the downstream distance increases. The attenuation resulting from forward motion appears to be concentrated in the low to middle frequency band. There is little attenuation resulting from forward motion for frequencies greater than 1500 Hz.

In Figs. 5a and 5b we show time histories of the normal velocities (v) at the panel centers for panels 1 and 2 (Fig. 5a) and panels 3 and 4 (Fig. 5b). In all cases there is a sustained long-time oscillation for v, even after the primary wave of incident $\tilde{p}$ has passed by the panel. This is probably a result of the low level of damping of the panels, i.e., a persistence of the initial pulse combined with panel excitation by disturbances shed from the instability waves. There appears to be little qualitative differences between the time histories for v as the downstream distance of the panel increases. Furthermore, the time histories with and without forward motion are similar. This suggests that much of the differences observed in the incident $\tilde{p}$ resulting from forward motion is not transmitted to the panel motion.

This is further seen by analysis of the spectrum of v. The velocity spectra exhibits rather discrete spectral bands, similar to those shown in Ref. 25. The panels act as filters to convert the broadband incident $\tilde{p}$ into relatively discrete spectral bands. The peak frequencies appear to be fairly insensitive to both panel location and forward motion. There is enhanced low-frequency content for the most downstream panel, panel 4. There is a residual effect of the starter pulse in the panel response resulting from the low damping of the panels.

In Fig. 5c we plot v along each panel for different values of t, with $7 \leq t \leq 10$. The predominant effect is that of waves propagating in both directions along each panel and reflecting from the clamped edges. The dark spots on the figures correspond to space–time locations where right-moving and left-moving waves intersect. Generally these intersections occur with a phase lag from panel to panel, indicating the convection of disturbances along the panel array. This is particularly noticeable in comparing panels 2, 3, and 4. Because of the restriction to a specific time window, this figure is most useful for assessing panel response in the mid- and high-frequency range. Low-frequency responses would not be brought out in these figures. Also note that each figure is internally scaled so that amplitude effects from panel to panel are not illustrated. Corresponding figures for the static computation (not shown) are qualitatively similar, confirming the conclusions drawn from the more detailed Figs. 5a and 5b that differences in incident $\tilde{p}$ resulting from forward motion are manifested primarily in the amplitude of the low-frequency panel response.

Examination of $\tilde{p}$ directly behind the panels (transmitted $\tilde{p}$) indicated features of both the incident $\tilde{p}$ and v. There is an initial disturbance corresponding to the incident pressure wave and a long-time

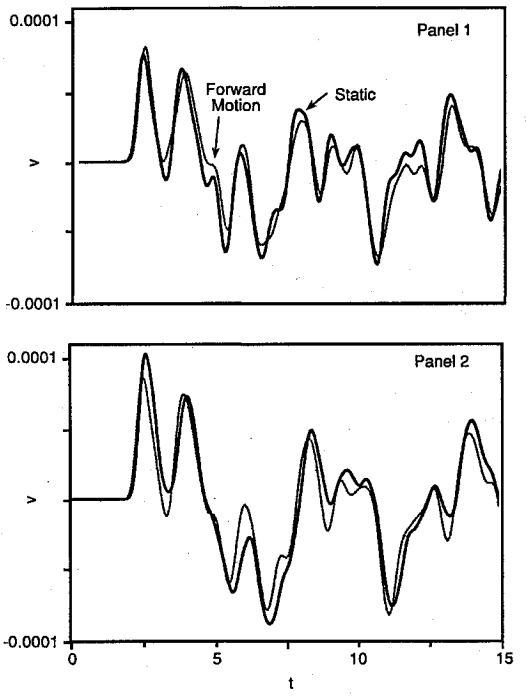

Fig. 5a Time history of v at centers of panels 1 and 2, with and without forward motion.

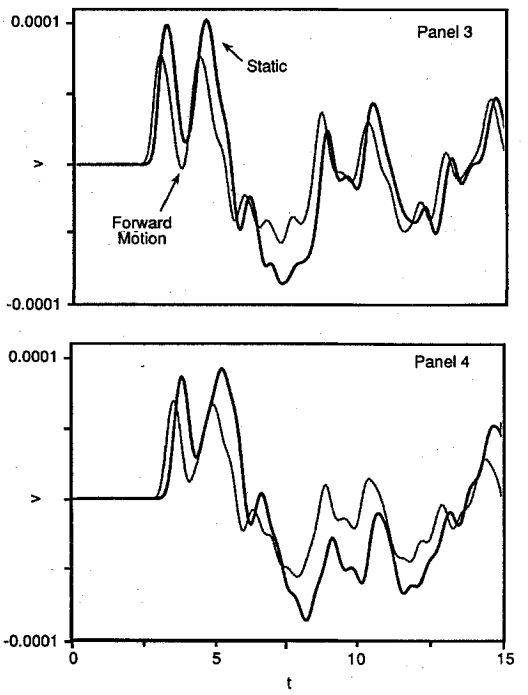

Fig. 5b Time history of v at centers of panels 3 and 4, with and without forward motion.

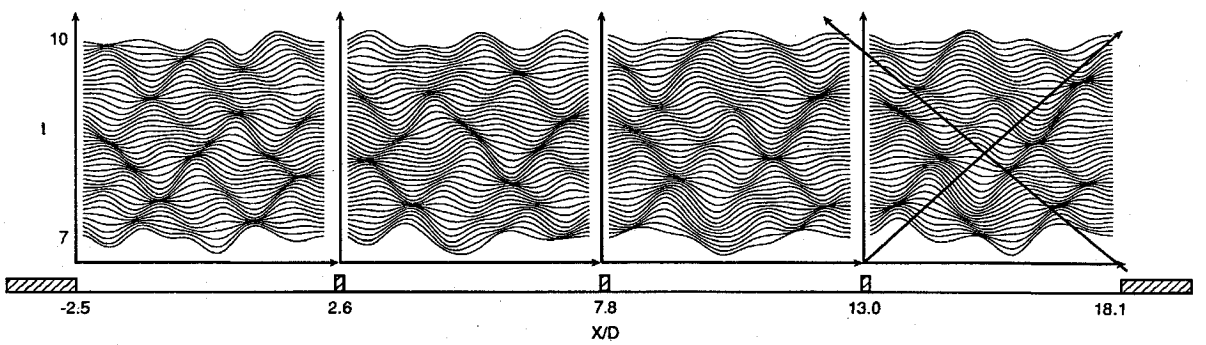

Fig. 5c $v(x, t)$ for $7 \leq t \leq 10$ along each panel. Computation with forward motion.

sustained response. This response is largely a result of the low damping of the panels, although the downstream panels, particularly panel 4, show evidence of late arrivals generated from instability waves.

The amplitude of the primary disturbance is slightly delayed and enhanced for panel 1, consistent with the behavior of the incident pressure in the jet domain, whereas for the other panels the incident wave for the computation without forward motion arrives later and is larger than the corresponding wave with forward motion. Thus these effects of forward motion are transmitted into the radiation domain. There is a noticeable attenuation in the amplitude of the pressure disturbances for panel 4 with forward motion. This may be a result of the enhanced low-frequency forcing of panel 4 for the static jet.

Examination of the spectral content of the transmitted $\tilde{p}$ indicates that the spectrum is composed of discrete frequency bands in contrast to the incident $\tilde{p}$, again illustrating the role of the panels as a filter to convert the broadband incident pressure into discrete frequency bands. In the low-frequency range, the characteristic frequencies of the bands appear to be relatively insensitive to the panel location or to whether there is forward motion or not. There is a large low-frequency response for panel 4, which is significantly attenuated with forward motion.

In summary, these results demonstrate the following:

1) The panels act as filters converting broadband incident $\tilde{p}$ into relatively narrow spectral bands.

2) Panels located further downstream are excited at lower frequencies, since they are forced by sound emanating from the shear layer at low to midrange angles from the jet axis. This results in enhanced low-frequency response for these panels.

3) An important effect of forward motion is to attenuate the low-frequency forcing for panels further downstream. This results in a significant attenuation of the amplitude of the panel oscillation and radiation at low frequencies.

Acoustic Radiation from the Panels

We have computed the radiated $\tilde{p}$ for various x locations on a line $y = 18D$ (corresponding to 0.9 m) in the radiation domain. Results for three different x locations are shown in Fig. 6a. The results show a leading arrival, followed by sustained pressure disturbances, similar to the transmitted $\tilde{p}$. There is a strong attenuation for upstream locations, indicating a preferred beaming of the radiated pressure in downstream directions. The convective effect of forward motion is

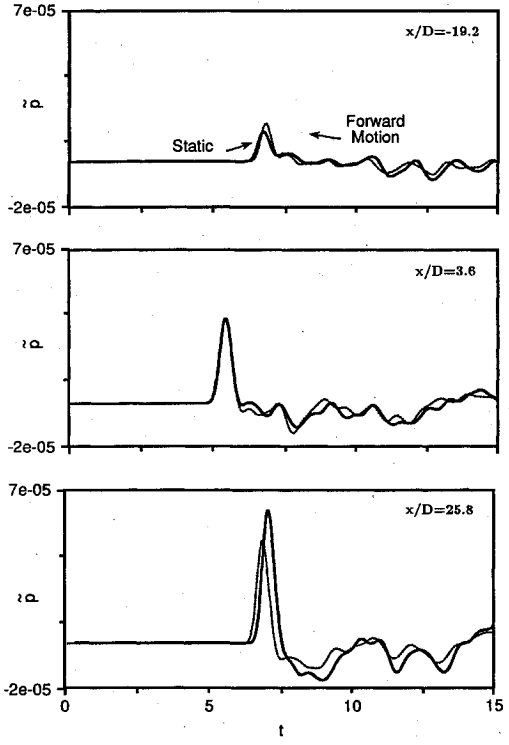

Fig. 6a Time history of $\tilde{p}$ in the radiation domain at $y = 18D$ at three different values of x, with and without forward motion.

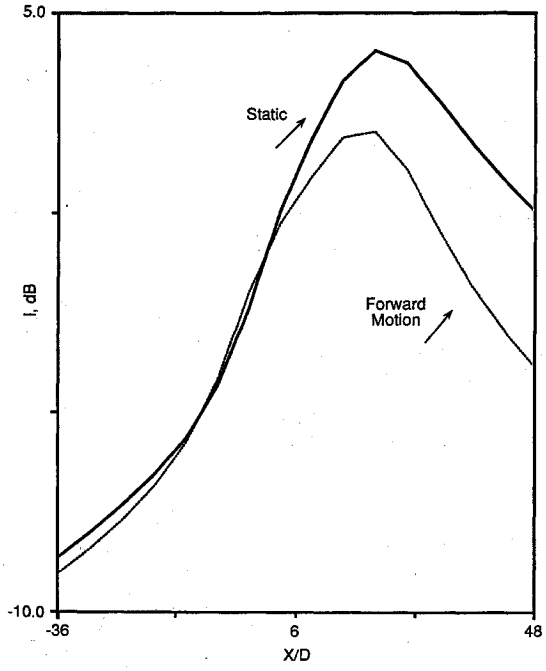

Fig. 6b Time-integrated intensity of pressure in radiation domain along the line $y = 18D$, with and without forward motion.

apparent in comparing the arrival times of the primary wave for the three locations. With forward motion there is a delay for the upstream location, no noticeable time lag or advance for the central location (we refer to this as the vertical location), and an earlier arrival for the downstream location. We also note that forward motion results in a slightly greater response upstream and a significant attenuation downstream, analogous to properties in the jet domain. There is virtually no difference in level for the vertical response. We note that these properties are transmitted via the panel radiation, as there is no forward motion in the radiation domain.

The upstream response is significantly smaller than the vertical or the downstream response, indicating a preferred downstream beaming of the radiated sound. This is true for both the static jet and the jet in forward motion. Forward motion reduces the downstream sound in the radiation domain. These results are further shown in Fig. 6b, where the total integrated intensity is plotted as a function of x along the line $y = 18D$. The data are expressed in decibels and normalized to 0 dB for the vertical location with no forward motion. We note that these data are presented along a line, so that there is an effect of cylindrical decay for large values of x; however, the preferred downstream beaming is apparent, as is the attenuation due to forward motion.

In summary:

1) Convective properties of the forward motion are transmitted to the radiation domain via transmission through the panels.

2) In both cases there is a preferred downstream beaming of sound in the radiation domain.

3) Forward motion significantly attenuates the radiated pressure in downstream directions (i.e., reduces but does not eliminate this preferred beaming).

Overall Flowfield

In Fig. 7 we show the pressure field in both the jet domain and the radiation domain at a fixed instant of time ($t = 11.3$) for the static computation. On the scale of the contour levels, an analogous plot for the forward-motion computation would be qualitatively similar. The figure shows a complex wave pattern, involving acoustic waves in both the radiation and jet domains together with slowly moving instability waves in the jet domain. Examination of the radiation domain shows propagation of high frequencies, characterized by closely spaced contours, upstream, whereas the pressure field downstream is primarily low-frequency (less dense contour distribution). Comparison with analogous data with forward motion (not shown) indicates a more pronounced radiation downstream.

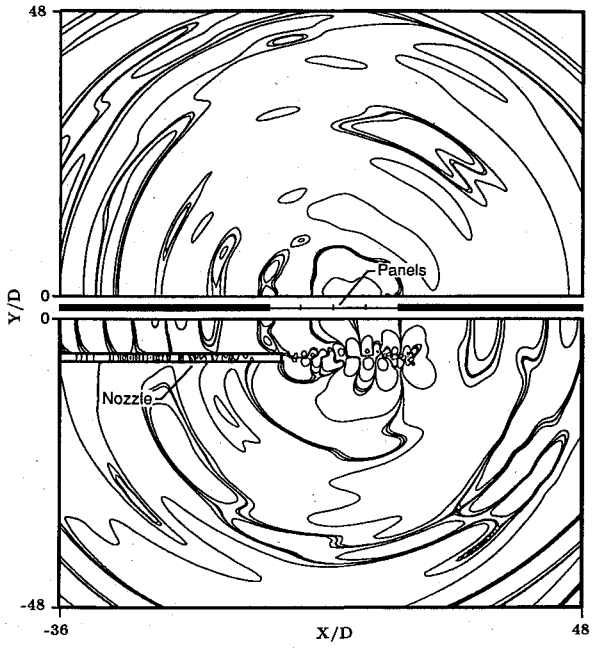

Fig. 7 Contours of $\tilde{p}$ for static computation, nondimensional time 11.3.

An important feature of the jet is the large-scale structure propagating along the jet axis. This structure is more pronounced and better defined than for the computation with forward motion, indicating the stabilizing effect of forward motion. The large-scale structure travels faster in the computation with forward motion, thus indicating that convection affects the speed of the instability waves. The generation of acoustic waves from this structure and from the nozzle lip can also be seen.

Conclusions

The far-field sound radiation is heavily influenced by the forward motion. There is an attenuation of sound downstream, while a forward arc amplification is observed upstream. These properties are apparent also in the incident pressure on the panels. The incident pressure is relatively broadband; however, low frequencies become more dominant for more downstream panels. There is a continual long-time excitation of the panels resulting from sound generated from instability-wave sources in the jet.

The panels act as filters converting the broadband incident $\tilde{p}$ to relatively narrow spectral bands. The panel response is sustained, because of the low damping and the continual excitation by instability-wave-generated sound. The peak frequencies appear to be insensitive to panel location and to forward motion. The amplitude of the low frequencies increases with downstream distance from the panel. Forward motion reduces the amplitude of low frequencies downstream. The radiated $\tilde{p}$ exhibits convection effects similar to the jet domain. There is a significant low-frequency beaming of sound, which is reduced by the forward motion.

Acknowledgments

A. Bayliss was partially supported by NASA Langley Research Center under Contracts NAS1-18605 and NAS1-19480 while in residence at Institute for Computer Applications in Science and Engineering. Additional support was provided by National Science Foundation Grants MMS 91-02981 and DMS 93-01635. J. L. McGreevy and C. C. Fenno Jr. were supported by NASA Langley Research Center while in residence under National Research Council Postdoctoral Research Associateship Awards. The authors thank T. D. Norum for helpful discussions and comments.

References

[1]Bauer, F., Maestrello, L., and Ting, L., "Acoustic Field in Unsteady Moving Media," *Journal of the Acoustical Society of America* (to be published).

[2]Bayliss, A., and Maestrello, L., "Simulation of Instabilities and Sound Radiation in a Jet," *AIAA Journal*, Vol. 19, 1981, pp. 835–841.

[3]Bayliss, A., Maestrello, L., and Turkel, E., "On the Interaction of a Sound Pulse with the Shear Layer of an Axisymmetric Jet, III: Non-Linear Effects," *Journal of Sound and Vibration*, Vol. 107, 1986, pp. 167–175.

[4]Bayliss, A., and Turkel, E., "Radiation Boundary Conditions for Wave-Like Equations," *Communications on Pure and Applied Mathematics*, Vol. 33, 1980, pp. 707–725.

[5]Bayliss, A., and Turkel, E., "Far-Field Boundary Conditions for Compressible Flows," *Journal of Computational Physics*, Vol. 48, 1982, pp. 182–199.

[6]Bechert, D. W., and Pfizenmaier, E., "On the Amplification of Broadband Jet Noise by Pure Tone Excitation," *Journal of Sound and Vibration*, Vol. 43, 1975, pp. 581–587.

[7]Broze, G., and Hussain, F., "Nonlinear Dynamics of Forced Transitional Jets: Periodic and Chaotic Attractors," *Journal of Fluid Mechanics*, Vol. 263, 1994, pp. 93–132.

[8]Bushell, K. W., "Measurement and Prediction of Jet Noise in Flight," AIAA Paper 75-461, March 1975.

[9]Crow, S., and Champagne, F., "Orderly Structure in Jet Turbulence," *Journal of Fluid Mechanics*, Vol. 48, 1971, pp. 457–591.

[10]Dowell, E. H., "Generalized Aerodynamic Forces on a Flexible Plate Undergoing Transient Motion is a Shear Flow with an Application to Panel Flutter," *AIAA Journal*, Vol. 9, 1971, pp. 834–841.

[11]Drevet, P., Duponchel, J. P., and Jacques, J. R., "The Effect of Flight on Jet Noise as Observed on the Bertin Aérotrain," *Journal of Sound and Vibration*, Vol. 54, 1977, pp. 173–201.

[12]Ffowcs Williams, J. E., "The Noise from Turbulence Convected at High Speed," *Philosophical Transactions of the Royal Society of London*, Vol. A255, 1963, pp. 469–503.

[13]Frendi, A., Maestrello, L., and Bayliss, A., "Coupling Between a Supersonic Boundary Layer and a Flexible Structure," *AIAA Journal*, Vol. 31, No. 4, 1993, pp. 708–713.

[14]Gottlieb, D., and Turkel, E., "Dissipative Two–Four Methods for Time-Dependent Problems," *Mathematics of Computation*, Vol. 30, 1976, pp. 703–723.

[15]Hayder, M. E., and Turkel, E., "Nonreflecting Boundary Conditions for Jet Flow Computations," *AIAA Journal*, Vol. 33, No. 12, 1995, pp. 2264–2270.

[16]Hoff, C., and Pahl, P. J., "Development of an Implicit Method with Numerical Dissipation from a Generalized Single-Step Algorithm for Structural Dynamics," *Computer Methods in Applied Mechanics and Engineering*, Vol. 67, 1988, pp. 367–385.

[17]Huerre, P., and Monkewitz, P. A., "Local and Global Instabilities in Spatially-Developing Flows," *Annual Review of Fluid Mechanics*, Vol. 22, 1990, pp. 473–537.

[18]Kibens, V., "Discrete Noise Spectrum Generated by an Acoustically Excited Jet," *AIAA Journal*, Vol. 18, 1980, pp. 434–441.

[19]Lighthill, M. J., "On Sound Generated Aerodynamically—I, General Theory," *Proceedings of the Royal Society of London*, Vol. A222, 1954, pp. 1–32.

[20]Lilley, G. M., "Theory of Turbulence Generated Jet Noise: Generation of Sound in a Mixing Region," U.S. Air Force TR AFAPL-TR-72-53, IV, Wright–Patterson AFB, OH, 1972.

[21]Maestrello, L., "Acoustic Energy Flow from Subsonic Jets and Their Mean and Turbulent Flow Structure," Ph.D. Thesis, Institute of Sound and Vibration Research, Univ. of Southampton, England, UK, 1975.

[22]Maestrello, L., "Control-Nonlinear-Nonstationary Structural Response and Radiation Near a Supersonic Jet," *AIAA Journal*, Vol. 32, 1994, pp. 1367–1375.

[23]Maestrello, L., Bayliss, A., and Turkel, E., "On the Interaction of a Sound Pulse with the Shear Layer of an Axisymmetric Jet," *Journal of Sound and Vibration*, Vol. 74, 1981, pp. 281–301.

[24]Mankbadi, R. R., Hayder, M. E., and Povinelli, L. A., "Structure of Supersonic Jet Flow and Its Radiated Sound," *AIAA Journal*, Vol. 32, No. 5, 1994, pp. 897–906.

[25]McGreevy, J. L., Bayliss, A., and Maestrello, L., "Interaction of Jet Noise with a Nearby Panel Assembly," *AIAA Journal*, Vol. 33, No. 4, 1995, pp. 577–585.

[26]Michalke, A., "Survey on Jet Instability Theory," *Progress in Aerospace Sciences*, Vol. 21, 1984, pp. 159–199.

[27]Michalke, A., and Hermann, G., "On the Inviscid Instability of a Circular Jet with External Flow," *Journal of Fluid Mechanics*, Vol. 114, 1982, pp. 343–359.

[28]Michalke, A., and Michel, U., "Prediction of Jet Noise in Flight from Static Tests," *Journal of Sound and Vibration*, Vol. 67, 1979, pp. 341–367.

[29]Norum, T. D., and Shearin, J. G., "Effects of Simulated Flight on the Structure of Underexpanded Jets," NASA TP 2308, 1984.

[30]Ribner, H. S., "Dryden Lecture Perspectives on Jet Noise," *AIAA Journal*, Vol. 19, 1981, pp. 1513–1526.

[31]Vlasov, Y. V., and Ginevsky, A. S., "Generation and Suppression of Turbulence in an Axisymmetric Turbulent Jet in the Presence of an Acoustic Influence," NASA-TT-F-15721, 1974 (translated from Russian).

[32]Way, D. J., and Francis, E. M., "The Simulation of Flight Effects on Jet Noise Using Co-Flowing Air Streams," AIAA Paper 77-1305, Oct. 1977.